Article

SOURCE DATA TRANSPARENT PROCESS

EMBO reports

Mcrs1 regulates G2/M transition and spindle assembly during mouse oocyte meiosis

Jia-Qian Ju, Zhen-Nan Pan, Kun-Huan Zhang, Yi-Ming Ji, Jing-Cai Liu & Shao-Chen Sun*

Abstract

Microspherule protein 1 (Mcrs1) is a component of the nonspecific lethal (NSL) complex and the chromatin remodeling INO80 complex, which participates in transcriptional regulation during mitosis. Here, we investigate the roles of Mcrs1 during female meiosis in mice. We demonstrate that Mcrs1 is a novel regulator of the meiotic G2/M transition and spindle assembly in mouse oocytes. Mcrs1 is present in the nucleus and associates with spindle poles and chromosomes of oocytes during meiosis I. Depletion of Mcrs1 alters HDAC2-mediated H4K16ac, H3K4me2, and H3K9me2 levels in nonsurrounded nucleolus (NSN)-type oocytes, and reduces CDK1 activity and cyclin B1 accumulation, leading to G2/M transition delay. Furthermore, Mcrs1 depletion results in abnormal spindle assembly due to reduced Aurora kinase (Aurka and Aurkc) and Kif2A activities, suggesting that Mcrs1 also plays a transcription-independent role in regulation of metaphase I oocytes. Taken together, our results demonstrate that the transcription factor Mcrs1 has important roles in cell cycle regulation and spindle assembly in mouse oocyte meiosis.

Keywords G2/M transition; Mcrs1; meiosis; oocyte; spindle
Subject Categories Cell Cycle
DOI 10.15252/embr.202256273 | Received 11 October 2022 | Revised 24 February 2023 | Accepted 1 March 2023 | Published online 23 March 2023
EMBO Reports (2023) 24: e56273

Introduction

Female fertility requires high-quality oocytes (Richani & Gilchrist, 2018). Oocytes present in ovarian follicles are arrested at the first meiotic prophase, which is also known as the germinal vesicle (GV) stage (Tan *et al*, 2009). Arrested oocytes accumulate many transcripts and proteins to allow them to progress through meiosis and to support early embryonic development, and there is almost no transcriptional activity once oocytes enter meiosis (Inoue *et al*, 2008). Chromatin in the GV of mouse oocytes undergoes extensive remodeling and posttranslational modifications, which are crucial for transcriptional regulation and remodeling of the oocyte genome before meiosis resumes (De La Fuente, 2006; Kang & Han, 2011). Oocytes that are transcriptionally active can be identified by the presence of decondensed chromatin, called the nonsurrounded nucleolus (NSN) configuration, while those that have completed this transcription are characterized by a tightly condensed chromatin ring surrounding the nucleolus, called the surrounded nucleolus (SN) configuration (Miyara *et al*, 2003). This synthesis and storage of transcripts prior to transcriptional silencing is essential for oocytes to attain the ability to undergo meiosis, known as meiotic resumption or the G2/M transition. Without it, inhibition of transcriptional activity in oocytes may trigger defects in their subsequent growth and maturation. Meiotic resumption is morphologically characterized by germinal vesicle breakdown (GVBD), the initial stage of oocyte maturation (Schmitt & Nebreda, 2002). This process is regulated by various pathways, which act in concert to activate the major regulator maturation promotion factor (MPF), which is composed of cyclin-dependent kinase 1 (CDK1) and its co-activator cyclin B1 (Sun *et al*, 2009). Maturation promotion factor is inactive when GV oocytes are arrested at prophase I (Holt *et al*, 2013). In response to a surge of gonadotropin, levels of cAMP rapidly drop, causing inactivation of protein kinase A, which results in the activation of CDK1 due to its decreased Wee1B-mediated inhibitory phosphorylation at Thr14 and Tyr15 (Han *et al*, 2005). Active CDK1 inhibits APC/C activity, allowing accumulation of cyclin B1 and subsequent activation of MPF (Holt *et al*, 2013). Meiotic progression is also closely associated with several epigenetic changes, which regulate the transcriptional activation of meiotic genes. For example, histone H4 is globally deacetylated during meiotic maturation (Kim *et al*, 2003), while H3 lysine 4 (H3K4; Hayashi *et al*, 2005) and lysine 9 (H3K9) methylation (Tachibana *et al*, 2007) dynamically changes during the early stages of meiosis.

After GVBD, oocytes undergo meiotic spindle assembly, chromosome segregation, cytokinesis, and polar body extrusion (PBE; Pan & Li, 2019), before arresting at metaphase of the second meiotic division until fertilization (MacLennan *et al*, 2015). It is essential that bipolar spindle assembly occurs correctly because errors in this process lead to mistakes in chromosome segregation and resultant DNA damage and aneuploidies (Mogessie *et al*, 2018). While spindle microtubules are primarily assembled from the centrosome in mitotic cells (Meunier & Vernos, 2016), centrosomes are eliminated before meiotic division in mouse oocytes (Szollosi

College of Animal Science and Technology, Nanjing Agricultural University, Nanjing, China
*Corresponding author. Tel/Fax: +86 25 84399092; E-mail: sunsc@njau.edu.cn

© 2023 The Authors

et al, 1972). The lack of canonical centrosomes in mouse oocytes leads to atypical modes of spindle assembly. (Mullen *et al*, 2019) Two distinct pathways cooperate to assemble bipolar spindles. Multiple acentriolar microtubule-organizing centers (aMTOCs) serve as a major site of microtubule nucleation and functionally replace centrosomes in mouse oocytes. aMTOCs contain several pericentriolar material components, including pericentrin (Carabatsos *et al*, 2000), γ-tubulin (Gueth-Hallonet *et al*, 1993) and its partner NEDD1 (Ma *et al*, 2010), and CEP192. To form a bipolar spindle, aMTOCs first fragment into numerous small MTOCs, which then cluster to form a bipolar spindle. Inhibition of MTOC fragmentation leads to spindle assembly defects, which delay chromosome congression and expose oocytes to the risk of aneuploidy (Clift & Schuh, 2015). In addition, chromatin-dependent mechanisms of microtubule nucleation and spindle assembly by the small GTPase Ran may also be important for acentrosomal spindle formation. Active GTP-bound Ran is generated by the chromatin-localized exchange factor RCC1 (Regulator of Chromosome Condensation 1; Petry, 2016). Thus, active Ran is present in a gradient around chromosomes, resulting in activation of spindle assembly factors such as TPX2, which participate in microtubule nucleation (Meunier & Vernos, 2016). Activation of Aurora kinase A (Aurka) by TPX2 is reportedly essential for Ran-stimulated spindle assembly in the presence or absence of centrosomes (Tsai & Zheng, 2005). In addition, Aurka regulates the MTOC number and spindle length, as well as recruitment of γ-tubulin to MTOCs during oocyte meiosis (Solc *et al*, 2012).

Microspherule protein 1 is an evolutionarily conserved protein originally identified in yeast (Ren *et al*, 1998). As a component of the nonspecific lethal (NSL) complex, Mcrs1 is involved in activation of ribosomal RNA transcription (Shimono *et al*, 2005) and regulation of RNA polymerase-II-dependent transcription (Andersen *et al*, 2010). Mcrs1 is also a core component of the INO80 chromatin modification complex, which plays a key role in regulating the cellular epigenetic landscape (Bao & Shen, 2007). Mcrs1 controls expression of bile acid transporter genes by evicting histone deacetylase 1 from its histone H3 anchoring sites and increasing histone acetylation (Garrido *et al*, 2022). In addition, Mcrs1 localizes to the minus ends of kinetochore microtubules during mitosis (Meunier & Vernos, 2011). The interaction between Mcrs1 and the mitotic kinase monopolar spindle 1 enhances recruitment of a kinesin motor to the minus ends of spindle microtubules in order to ensure accurate chromosome separation (Yang *et al*, 2019). Mcrs1 has also been reported to enhance microtubule stability and to interact with the key spindle assembly factor TPX2 (Meunier *et al*, 2015). Although Mcrs1 is involved in multiple biological processes during mitosis, its role during meiosis I in oocytes has not been elucidated.

Here, we investigated the function and regulation of Mcrs1 during oocyte meiosis and maturation using knockdown (KD) and rescue approaches. We demonstrated that Mcrs1 acts as a priming signal for meiotic cell cycle progression by mediating histone modifications and transcriptional regulation in NSN-type GV oocytes. Furthermore, we found that Mcrs1 localizes to spindle poles and cooperates with Aurora kinases to regulate spindle assembly during meiosis I in oocytes. These data provide the first evidence that Mcrs1 plays a role during mouse oocyte meiosis.

Results

Mcrs1 is essential for meiotic resumption and maturation in mouse oocytes

To explore the potential role of Mcrs1 in oocyte meiosis, we first determined its protein expression and subcellular localization at different developmental stages during mouse oocyte maturation. Western blotting demonstrated that Mcrs1 was expressed in oocytes throughout meiotic maturation (Fig 1A). To examine the subcellular localization of Mcrs1, GV oocytes were injected with RFP-Mcrs1 mRNA (750 ng/μl). Fluorescence microscopy revealed that Mcrs1 was predominantly present in the nucleus of GV oocytes, but accumulated at the meiotic spindle poles and chromosomes after GVBD (Fig 1B). Western blotting of RFP-Mcrs1 mRNA-injected GV oocytes demonstrated that RFP-Mcrs1 protein was expressed in oocytes for 2 h after microinjection (Fig 1C). To investigate the function of Mcrs1, siRNA was used to deplete Mcrs1 protein in oocytes. Immunoblotting and immunofluorescence microscopy with anti-Mcrs1 antibodies demonstrated that Mcrs1 protein was efficiently depleted by injection of Mcrs1 siRNA (Fig 1D and E). Examination of maturation of Mcrs1 siRNA-injected oocytes that had been cultured for 12 h showed that Mcrs1 depletion substantially perturbed first PBE. To exclude off-target effects, exogenous Mcrs1 was expressed in Mcrs1 siRNA-injected oocytes (Mcrs1-rescue oocytes). This restored the percentage of oocytes that underwent PBE to control levels (Control: 69.03 ± 1.17%; Mcrs1-KD: 40.42 ± 5.42%; Mcrs1-rescue: 62.48 ± 2.82%; Fig 1F and G). These data suggest that Mcrs1 is essential for oocyte meiotic progression. A relatively low percentage of Mcrs1-KD oocytes underwent GVBD after 12-h culture, indicating that Mcrs1 plays a role in the G2/M transition (Control: 80.17 ± 1.62%; Mcrs1-KD: 54.5 ± 3.59%; Mcrs1-rescue: 74.1 ± 1.78%; Fig 1F and G).

Mcrs1 regulates cyclin B1 accumulation and CDK1 activity for meiotic resumption in oocytes

To further explore the mechanism by which Mcrs1 affects meiotic resumption in oocytes, we observed GVBD at 1–3 h after release from IBMX, which stimulates GVBD. Upon release from IBMX, most Mcrs1-KD oocytes remained arrested at the GV stage and GVBD was severely delayed. This defect was rescued by supplementation of Mcrs1 mRNA, suggesting it was specifically due to Mcrs1 depletion and not an off-target effect (Fig 2A and B). To further investigate the reasons for the observed prophase I arrest, we investigated the two critical components of MPF, CDK1, and cyclin B1. To explore the interaction between CDK1/cyclin B1 and Mcrs1, co-immunoprecipitation (Co-IP) experiments were performed, and the results showed that cyclin B1 was present in Mcrs1 protein precipitates (Fig 2C). Meanwhile, examination of expression of CDK1 and its inhibitory phosphorylation at Tyr15 demonstrated that the CDK1 level was significantly lower and its level of phosphorylation was much higher in Mcrs1-KD oocytes than in control oocytes at 1 h following release from IBMX, indicating that CDK1 activity was inhibited in Mcrs1-KD oocytes (CDK1, Control: 1 vs. Mcrs1-KD: 0.59 ± 0.09; p-CDK1(Y15): Control: 1 vs. Mcrs1-KD: 2.4 ± 0.26; Fig 2D and E). The cyclin B1 level was significantly reduced in Mcrs1-KD oocytes (Control: 1 vs. Mcrs1-KD: 0.65 ± 0.02; Fig 2F). To verify these results, after 12-h KD with Mcrs1 siRNA, we used a Wee1 kinase inhibitor (WEE1-IN-4) to pharmacologically

 © 2023 The Authors

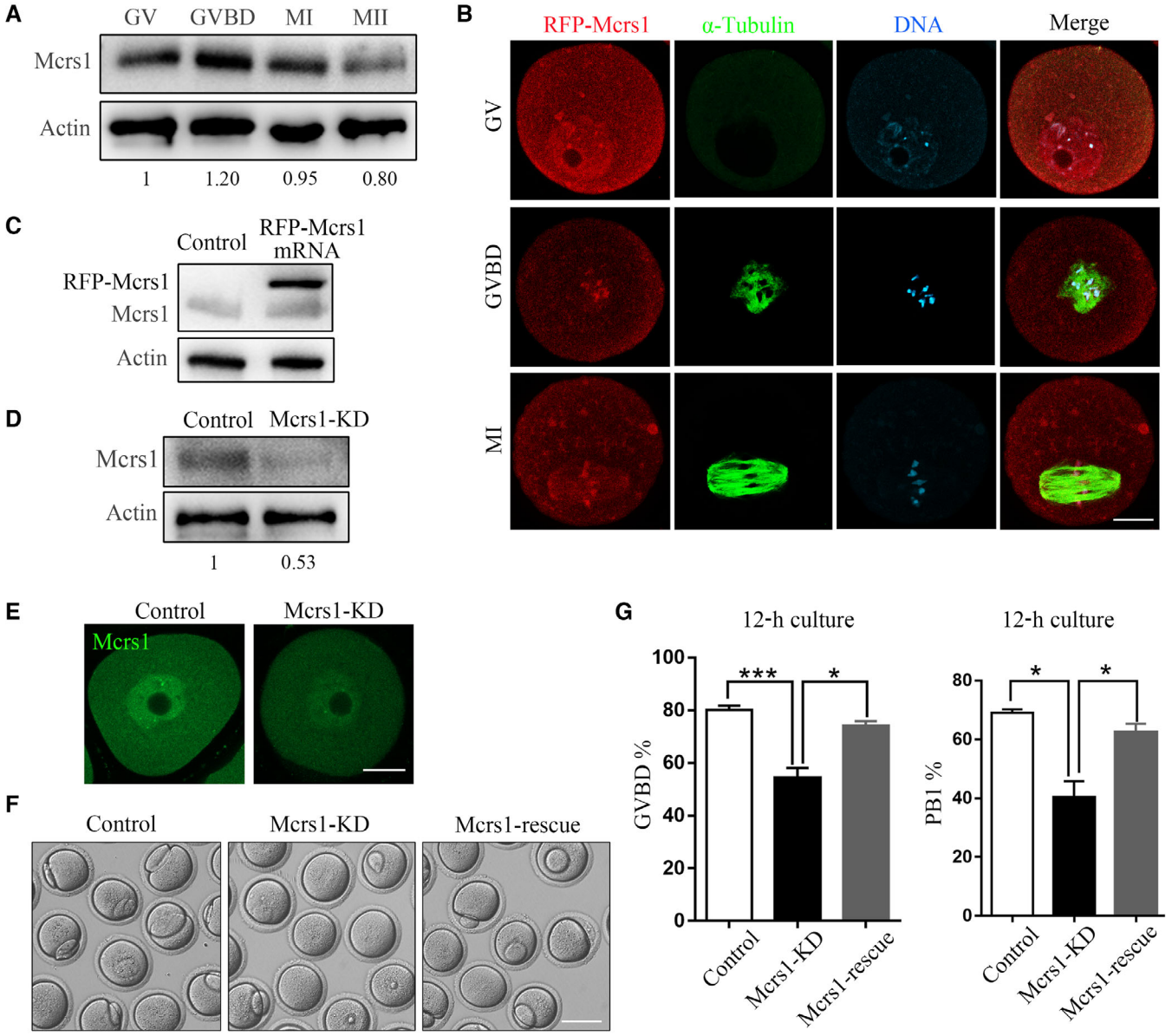

Figure 1. Mcrs1 depletion impairs progression of the meiotic cell cycle in oocytes.

A Western blotting of Mcrs1 at the GV (0 h), GVBD (4 h), MI (8 h), and MII (12 h) stages of mouse oocyte meiosis. The blots were probed with anti-Mcrs1 and anti-actin antibodies.

B Representative images of RFP-Mcrs1 localization during mouse oocyte meiosis. Mouse oocytes at different developmental stages were immunostained with an anti-α-tubulin antibody (green). The localization of RFP-Mcrs1 (red) was determined. DNA (blue) was counterstained with Hoechst 33342. Scale bar, 20 μm.

C Western blotting of Mcrs1 and β-actin in Mcrs1 mRNA-injected and control oocytes.

D Western blotting of Mcrs1 and β-actin in Mcrs1-KD and control oocytes.

E Immunofluorescence analysis of Mcrs1 in control and Mcrs1-KD oocytes. Scale bar, 20 μm.

F Representative images of the occurrence of GVBD and PBE in control, Mcrs1-KD, and Mcrs1-rescue (Mcrs1 siRNA + Mcrs1 mRNA) oocytes at 12 h following release from IBMX. Scale bar, 100 μm.

G Percentages of control ($n = 210$), Mcrs1-KD ($n = 182$), and Mcrs1-rescue ($n = 201$) oocytes that underwent GVBD and PBE. The bars are representing the mean ± SEM. The P-values were calculated using Student's t-test. GVBD%: ***$P = 0.0003$; *$P = 0.01$, PB1%: *$P = 0.03$; *$P = 0.02$.

Source data are available online for this figure.

activate CDK1 and verified its efficiency. WEE1-IN-4 effectively inhibited phosphorylation of CDK1 (Fig 2G). We also injected cyclin B1-GFP mRNA into oocytes arrested at the GV stage and cultured these oocytes for 3 h to allow protein expression (Fig 2H). WEE1-IN-4 effectively inhibited phosphorylation of CDK1 to rescue GVBD failure in Mcrs1-KD oocytes (Fig 2I). Overexpression of cyclin B1-GFP also

© 2023 The Authors

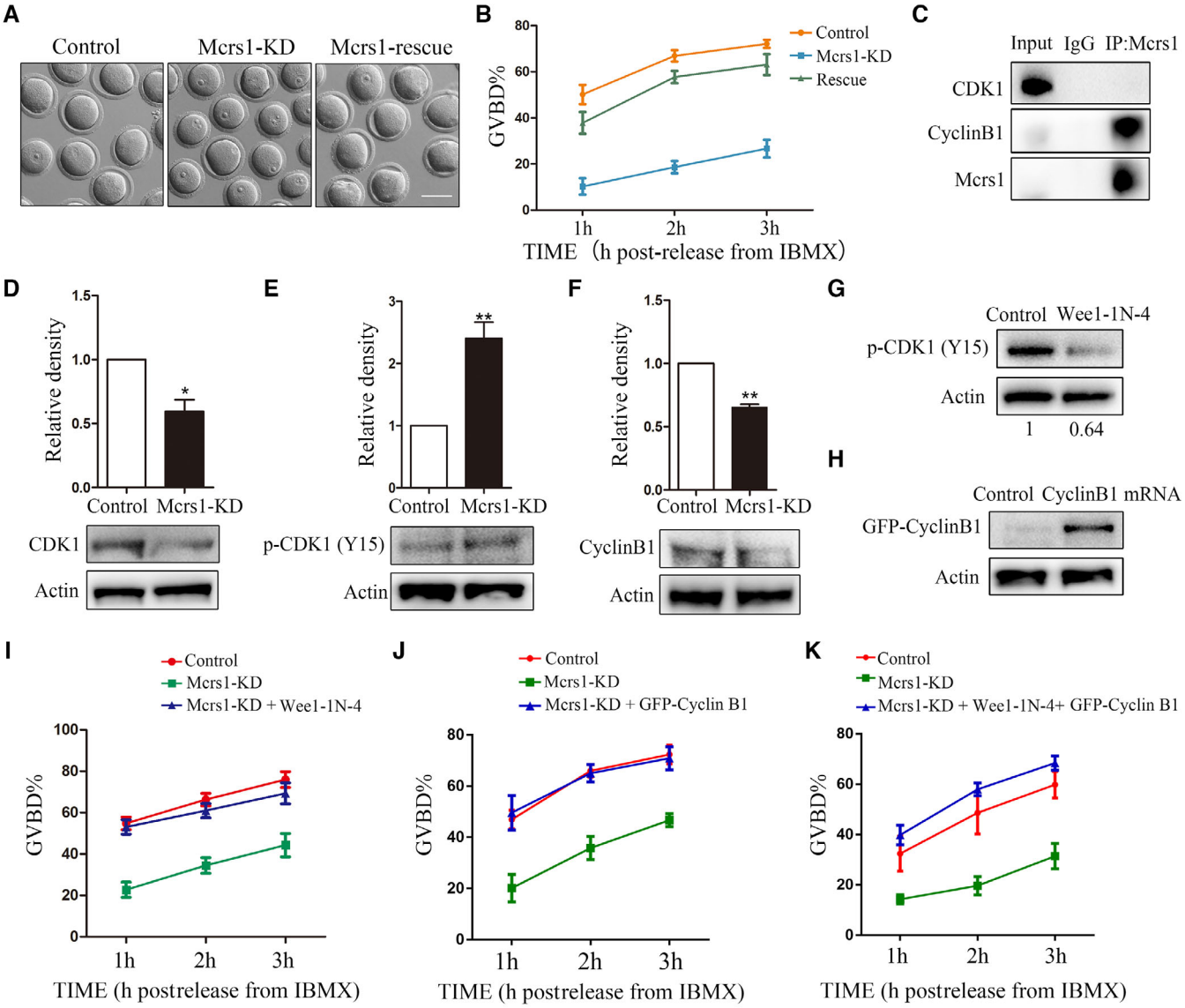

Figure 2. Depletion of Mcrs1 delays GVBD by impairing CDK1 activity and accumulation of cyclin B1 in oocytes.

A Representative images of the occurrence of GVBD in control, Mcrs1-KD, and Mcrs1-rescue (Mcrs1 siRNA + Mcrs1 mRNA) oocytes at 3 h following release from IBMX. Scale bar, 100 μm.

B The incidence of GVBD at 1, 2, and 3 h post-IBMX release in control ($n = 155$), Mcrs1-KD ($n = 157$), and Mcrs1-rescue ($n = 150$) oocytes.

C Co-IP was performed with an anti-Mcrs1 antibody. The immunoblots of protein precipitates were probed with anti-CDK1 and anti-cyclin B1 antibodies.

D Expression levels of CDK1 in Mcrs1-KD and control oocytes. The bars represent the mean (± SEM) of 5 biological replicates. The *P*-values were calculated using Student's *t*-test. $^{*}P = 0.01$.

E Expression levels of p-CDK1(Y15) in Mcrs1-KD and control oocytes at 1 h following release from IBMX (200 oocytes per sample). The bars represent the mean (± SEM) of three biological replicates. The *P*-values were calculated using Student's *t*-test. $^{**}P = 0.006$.

F Expression levels of cyclin B1 in control and Mcrs1-KD oocytes at 1 h following release from IBMX (200 oocytes per sample). The bars represent the mean (± SEM) of three biological replicates. The *P*-values were calculated using Student's *t*-test. $^{**}P = 0.0042$.

G Protein levels of p-CDK1(Y15) in control and WEE1-IN-4-treated GV oocytes. The blots were probed with anti-p-CDK1(Y15) and anti-actin antibodies.

H Western blotting of GFP-cyclin B1 and β-actin in GFP-cyclin B1 mRNA-injected and control oocytes.

I The incidence of GVBD at 1, 2, and 3 h post-IBMX release in control oocytes ($n = 112$), Mcrs1-KD oocytes ($n = 98$), and Mcrs1-KD oocytes treated with 5 mM WEE1-IN-4 ($n = 102$).

J The incidence of GVBD at 1, 2, and 3 h post-IBMX release in control ($n = 123$), Mcrs1-KD ($n = 134$), and Mcrs1 siRNA + cyclin B1-GFP ($n = 95$) oocytes.

K The incidence of GVBD at 1, 2, and 3 h post-IBMX release in control ($n = 92$), Mcrs1-KD ($n = 97$), and Mcrs1 siRNA + cyclin B1-GFP oocytes treated with 5 mM WEE1-IN-4 ($n = 106$).

Source data are available online for this figure.

 © 2023 The Authors

rescued impaired GVBD after Mcrs1 depletion within 3 h (Fig 2J). Meanwhile, simultaneous overexpression of cyclin B1-GFP and treatment with WEE1-IN-4 better rescued GVBD failure in Mcrs1-KD oocytes (Fig 2K).

Mcrs1 is crucial for histone modifications and transcriptional regulation in GV oocytes

To explore the mechanism by which Mcrs1 affects meiotic resumption, we performed mass spectrometry analysis. This showed that Mcrs1 associated with multiple transcription-related proteins (Fig 3A). Therefore, we hypothesized that Mcrs1 is involved in transcriptional regulation in NSN-type oocytes during GV phase and affects cyclin expression and facilitates meiotic resumption. To label newly synthesized RNAs in GV oocytes, we incubated control and Mcrs1-KD oocytes with 100 μM 5-ethynyl uridine (EU) for 2 h and detected EU-tagged transcripts using a Cell-Light EU Apollo488 RNA Imaging Kit. The intensity of EU signals was lower in Mcrs1-KD oocytes than in control oocytes at the GV stage (NSN configuration). This difference was abrogated by supplementation of Mcrs1 mRNA, which excluded the possibility of off-target effects (Control: 19,026 ± 1,331 vs. Mcrs1-KD: 11,003 ± 682.5 vs. Mcrs1-rescue: 19,845 ± 1,248; Fig 3B). Therefore, depletion of Mcrs1 in oocytes downregulated transcriptional activity. Next, we investigated the levels of histone modifications involved in transcriptional regulation. We first examined the level of histone H3 lysine 4 dimethylation (H3K4me2), which is associated with transcriptional permissiveness in mammalian genomes, in GV oocytes. The fluorescence intensity of H3K4me2 signals was significantly lower in Mcrs1-KD oocytes than in control oocytes (Control: 9,461 ± 352 vs. Mcrs1-KD: 7,560 ± 261.6; Fig 3C). This was further verified by Western blotting, which showed that Mcrs1 KD significantly decreased H3K4me2 protein expression (Fig 3D). By contrast, as an important epigenetic mark associated with transcriptional repression, the level of histone H3 lysine 9 dimethylation (H3K9me2) was significantly higher in Mcrs1-KD oocytes than in control oocytes (Control: 10,321 ± 383 vs. Mcrs1-KD: 12,200 ± 430.2; Fig 3E). Histone acetylation, including histone H4 lysine 16 acetylation (H4K16ac), is associated with modifications of the higher order chromatin structure in the nucleosome, resulting in enhanced transcriptional activity. Immunofluorescence analysis revealed that the fluorescence intensity of H4K16ac signals was lower in Mcrs1-KD oocytes than in control oocytes at the GV stage (NSN configuration; Control: 12,143 ± 652.3 vs. Mcrs1-KD: 10,071 ± 585.3; Fig 3F). Conversely, the fluorescence intensity of signals of histone deacetylase 2 (HDAC2), a transcription repressor at promoter regions of target genes, was significantly higher in Mcrs1-KD oocytes than in control oocytes at the GV stage (Control: 14,337 ± 388 vs. Mcrs1-KD: 16,512 ± 436.3; Fig 3G). Mcrs1 depletion also prominently increased the protein level of HDAC2 (Fig 3H). In addition, immunoblots after Co-IP with an anti-Mcrs1 antibody revealed that HDAC2 was present in the protein precipitate (Fig 3I).

Mcrs1 is indispensable for meiotic spindle assembly and chromosome alignment in oocytes

Due to its localization pattern after GVBD, we hypothesized that Mcrs1 plays a regulatory role in spindle assembly during meiosis. Therefore, spindle structures after GVBD were observed in control and Mcrs1-KD oocytes. The fluorescence intensity and area of the spindle were significantly lower in Mcrs1-KD oocytes than in control oocytes (fluorescence intensity, Control: 1 vs. Mcrs1-KD: 0.66 ± 0.05; spindle area, 1 vs. Mcrs1-KD: 0.59 ± 0.03; Fig 4A and B). While control oocytes had formed metaphase I (MI) spindles after 8-h culture, a high percentage of Mcrs1-KD oocytes contained small spindles and microtubule "balls" (spindles whose length was less than one-third of the oocyte diameter were classified as small and a microtubule "ball" was a spherical spindle that was not bipolar) with weak immunofluorescence signals of α-tubulin (Control: 21.55 ± 4.06% vs. Mcrs1-KD: 63.79 ± 6.75% vs. Mcrs1-rescue: 40.68 ± 4.61%). A higher percentage of Mcrs1-KD oocytes than control oocytes had misaligned chromosomes (Control: 15.78 ± 2.094% vs. Mcrs1-KD: 48.09 ± 5.14% vs. Mcrs1-rescue: 31.79 ± 4.45%; Fig 4C and D). Next, to rule out the possibility that spindles failed to form in Mcrs1-KD oocytes due to the effects of CDK1 and cyclin B1 on the cell cycle, we overexpressed cyclin B1-GFP and performed treatment with WEE1-IN-4 in Mcrs1-KD oocytes. Neither rescued the defect in spindle assembly (Control: 19.91 ± 6.31% vs. Mcrs1-KD: 44 ± 6.80% vs. Mcrs1-KD±GFP-CCNB1: 44.94 ± 2.57% vs. Mcrs1-KD±WEE1-IN-4: 42.65 ± 5.35%; Fig 4E). However, expression of exogenous Mcrs1 rescued the spindle and chromosome defects. To quantitatively evaluate the phenotype, we measured the width of the spindle middle plate, which is the area occupied by condensed chromosomes, and the length of the spindle. The middle plate was significantly broader in Mcrs1-KD oocytes than in control oocytes, and the relative spindle length was significantly shorter in MI oocytes after Mcrs1 KD (C:S, Control: 0.34 ± 0.01 vs. Mcrs1-KD: 0.51 ± 0.04; S:L, Control: 0.43 ± 0.018 vs. Mcrs1-KD: 0.35 ± 0.004; Fig 4F). Histone H3 phosphorylated at Ser-10 (H3S10ph) is crucial for chromosome condensation. We compared the levels of H3S10ph between control and Mcrs1-KD oocytes that had been cultured for 8 h by performing immunofluorescence staining. The fluorescence intensity of H3S10ph signals was significantly lower in Mcrs1-KD oocytes than in control oocytes (Control: 9,821 ± 681.4 vs. Mcrs1-KD: 7,389 ± 692.9; Fig 4G). The MTOC-specific protein γ-tubulin is important for microtubule nucleation and spindle formation during mouse oocyte meiosis. We explored the effect of Mcrs1 KD on the localization of γ-tubulin. The number of γ-tubulin dots was significantly decreased, and γ-tubulin failed to concentrate at spindle poles in a high percentage of Mcrs1-KD oocytes (Control: 14 ± 5.70% vs. Mcrs1-KD: 38.43 ± 1.56%; Fig 4H). We detected acetylated tubulin by immunofluorescence staining. The fluorescence intensity of acetylated tubulin signals was significantly lower in Mcrs1-KD oocytes than in control oocytes (Control: 1 vs. Mcrs1-KD: 0.70 ± 0.02; Fig 4I).

Mcrs1 collaborates with Aurora kinases for spindle assembly in oocytes

The small spindles and microtubule "balls" in Mcrs1-KD oocytes are reminiscent of the phenotype caused by depletion of Aurora kinases, which are spindle assembly factors. Thus, we compared the levels of Aurka (Aurora A) and Aurkc (Aurora C) between control and Mcrs1-KD oocytes that had been cultured for 8 h by performing immunofluorescence staining and Western blotting. P-Aurka no longer accumulated at spindle poles and was irregularly distributed in

© 2023 The Authors

the cytoplasm in a high percentage of Mcrs1-KD oocytes (Control: 8.89 ± 1.69% vs. Mcrs1-KD: 45.76 ± 5.77%; Fig 5A). Similarly, the fluorescence intensity of p-Aurkc signals was significantly decreased in Mcrs1-KD oocytes (Control: 9,730 ± 432.6 vs. Mcrs1-KD: 7,352 ± 506.8; Fig 5B). This finding was confirmed by Western blotting (Fig 5C). Meanwhile, immunoblotting after co-IP with an anti-Mcrs1 antibody revealed that Aurka was present in the protein precipitate. In reciprocal experiments, Mcrs1 was observed in the protein precipitate after co-IP with an anti-Aurka antibody (Fig 5D), confirming that Mcrs1 interacts with Aurka in oocytes. For further

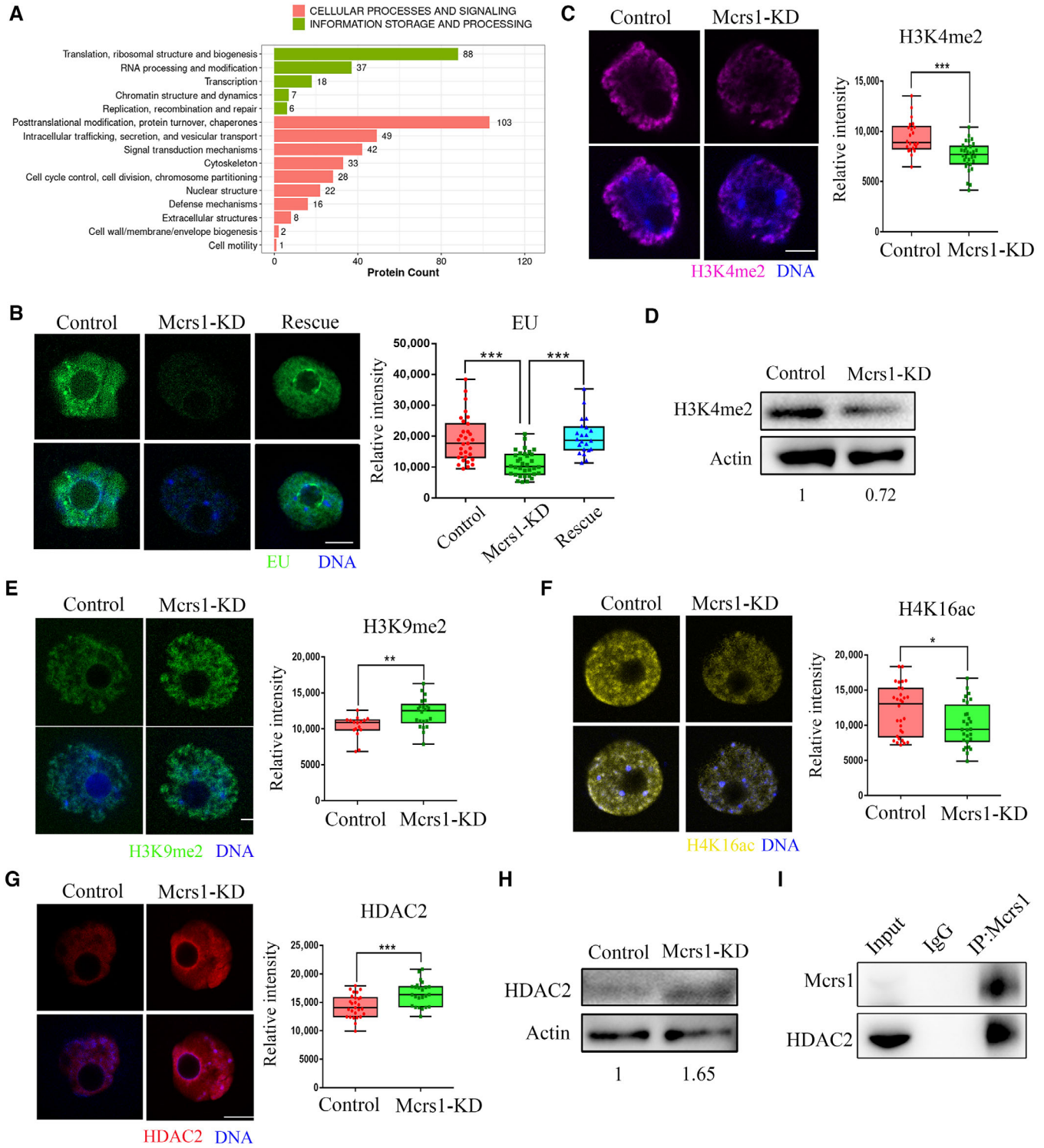

Figure 3.

© 2023 The Authors

Figure 3. Mcrs1 depletion impairs histone modifications and transcriptional regulation in GV oocytes.

A KGO analysis of Mcrs1-associated proteins by mass spectrometry.
B Detection of newly synthesized RNAs by EU incorporation in control, Mcrs1-KD, and Mcrs1-rescue GV oocytes. The scattergram shows the relative fluorescence intensity of EU in control ($n = 43$), Mcrs1-KD ($n = 52$), and Mcrs1-rescue ($n = 30$) GV oocytes. Scale bar, 10 μm. ***$P = 0.0001$.
C Immunofluorescence analysis of H3K4me2 in control and Mcrs1-KD oocytes. Scale bar, 10 μm. Relative fluorescence intensity of H3K4me2 signals in control ($n = 26$) and Mcrs1-KD ($n = 30$) GV oocytes. ***$P = 0.0001$.
D Protein levels of H3K4me2 in control and Mcrs1-KD GV oocytes. The blots were probed with anti-H3K4me2 and anti-actin antibodies.
E Immunofluorescence analysis of H3K9me2 in control and Mcrs1-KD oocytes. Scale bar, 10 μm. Relative fluorescence intensity of H3K9me2 signals in control ($n = 29$) and Mcrs1-KD ($n = 22$) GV oocytes. **$P = 0.0035$.
F Immunofluorescence analysis of H4K16ac in control and Mcrs1-KD oocytes. Scale bar, 10 μm. Relative fluorescence intensity of H4K16ac signals in control ($n = 30$) and Mcrs1-KD ($n = 28$) GV oocytes. *$P = 0.022$.
G Immunofluorescence analysis of HDAC2 in control and Mcrs1-KD oocytes. Scale bar, 10 μm. Relative fluorescence intensity of HDAC2 signals in control ($n = 27$) and Mcrs1-KD ($n = 24$) GV oocytes. ***$P = 0.0005$.
H Protein levels of HDAC2 in control and Mcrs1-KD GV oocytes. The blots were probed with anti-HDAC2 and anti-actin antibodies.
I Co-IP was performed with an anti-Mcrs1 antibody. The immunoblots of protein precipitates were probed with anti-HDAC2 and anti-Mcrs1 antibodies.

Data information: The central band are representing mean. The boxes are representing mean ± SEM and the whiskers are representing Mix to Max. The *P*-values were calculated using unpaired *t*-test.
Source data are available online for this figure.

verification, GFP-Aurka was injected into Mcrs1-KD oocytes (Aurka-rescue). Notably, GFP-Aurka rescued PBE failure and spindle defects in Mcrs1-KD oocytes (Fig 5E and F). This was confirmed by statistical analysis of the percentages of oocytes that underwent PBE and displayed spindle defects (PBE, Control: 69.03 ± 1.17% vs. Mcrs1-KD: 40.42 ± 5.42% vs. Aurka-rescue: 57.5 ± 3.82%; spindle defects, Control: 4.533 ± 2.50% vs. Mcrs1-KD: 37.62 ± 3.22% vs. Aurka-rescue: 22.61 ± 1.63%; Fig 5G and H). Collectively, these results indicate that Aurka is the downstream effector of Mcrs1 during meiotic spindle assembly in oocytes. Next, we investigated the expression and localization of TPX2 and Kif2A, which are an activator and downstream protein of Aurka, respectively. The protein level of Kif2A was significantly lower in Mcrs1-KD oocytes than in control oocytes, and Kif2A failed to accumulate at spindle poles in a high percentage of Mcrs1-KD oocytes (Control: 15.93 ± 4.00% vs. Mcrs1-KD: 53.59 ± 2.06%; Fig 5I and K). However, the localization and protein level of TPX2 were not significantly changed in Mcrs1-KD oocytes (Control: 8387 ± 647.5 vs. Mcrs1-KD: 8603 ± 662; Fig 5J and L).

Discussion

Microspherule protein 1 reportedly functions in transcriptional regulation, cellular proliferation, senescence induction, and mitotic progression in different mitotic models. In the present study, we explored the functional roles of Mcrs1 during mouse oocyte meiosis, a cell model with low transcriptional activity, and the underlying mechanisms. We showed that Mcrs1-mediated histone modifications were essential for transcriptional regulation in NSN-type GV oocytes, which further determined meiotic resumption. In addition, Mcrs1 regulated microtubule nucleation and spindle assembly by activating Aurora kinases during mouse oocyte meiosis (Fig 6).

Our findings showed that the subcellular localization patterns of Mcrs1 during oocyte meiosis and mitosis differ. In mitotic cells, Mcrs1 accumulates in the nucleus during interphase and translocates to the minus ends of kinetochore microtubules following nuclear envelope breakdown (Petry & Vale, 2011). In addition, it has been reported that Mcrs1 is more concentrated in the nucleus of embryos by the four-cell stage and is indispensable for epiblast development (Cui *et al*, 2020). However, different with the mitosis of embryo development, oocyte maturation is meiosis. Mcrs1 is found to be transcription regulators in mitosis, while during oocyte maturation, there is almost no transcription activities, which makes the oocyte a unique and valuable model to study. And our data suggest that Mcrs1 in oocytes has distinct functions in meiosis. We found that Mcrs1 was essential for the G2/M transition during oocyte meiosis, but it has not been reported to play such a role in mitosis. We showed that cyclin B1 might interact with Mcrs1, indicating the potential relationship between Mcrs1 and cyclin B1, and depletion of Mcrs1 in oocytes delayed meiotic resumption due to perturbation of CDK1 activity and failure of cyclin B1 accumulation, but meiotic resumption was restored by expression of exogenous cyclin B1 and activation of CDK1 using a Wee1 inhibitor. CDK1 and cyclin B1, which are components of MPF, reportedly participate in regulation of the meiotic G2/M transition (Schmitt & Nebreda, 2002). These results indicated that Mcrs1 regulated MPF activity and ultimately affected G2/M transition. In addition to the regulation of MPF activity, meiotic progression is accompanied by chromatin remodeling and epigenetic changes (Sasaki & Matsui, 2008). For example, depletion of the CxxC zinc finger protein Cfp1, a major mediator of histone H3 lysine 4 trimethylation, delays meiotic resumption and perturbs spindle assembly (Sha *et al*, 2018). LSD1, a lysine demethylase, reportedly regulates H3K4me2 in mouse oocytes and is essential for meiotic progression, and its deletion results in precocious resumption of meiosis and spindle/chromosomal abnormalities (Kim *et al*, 2015). Depletion of Setdb1, a H3K9 methyltransferase, delays meiotic resumption and alters the dynamics of chromatin condensation in mouse oocytes (Eymery *et al*, 2016). In addition, the chromatin remodeler Snf2h regulates meiosis-related genes, which in turn affects MPF activity and meiotic resumption (Zhang *et al*, 2020). However, depletion of these epigenetic regulators only delays meiotic resumption, but does not completely block GVBD. This is similar to our observation that depletion of Mcrs1 delayed meiotic resumption in oocytes. Mcrs1 is a component of the NSL complex, which is involved in transcriptional regulation (Sheikh *et al*, 2019), and of the INO80 complex, which plays an important role in chromatin remodeling (Jin *et al*, 2005). As expected, our results showed that Mcrs1 was involved in the regulation of transcription and histone modifications

© 2023 The Authors

including methylation (H3K9me2 and H3K4me2) and acetylation (H4K16ac) in GV oocytes. We hypothesized that since transcription is greatly inhibited during the conversion of GV oocytes from the NSN configuration to the SN configuration, depletion of Mcrs1 disrupts the transcriptional balance in NSN-type oocytes, which induces changes in histone epigenetic modifications. Notably, we found that Mcrs1 interacted with the deacetylase HDAC2, and KD of Mcrs1 increased the HDAC2 level, which inhibited histone acetylation in GV oocytes. HDAC2 reportedly regulates transcription and apoptosis during mouse oocyte development (Ma *et al*, 2012).

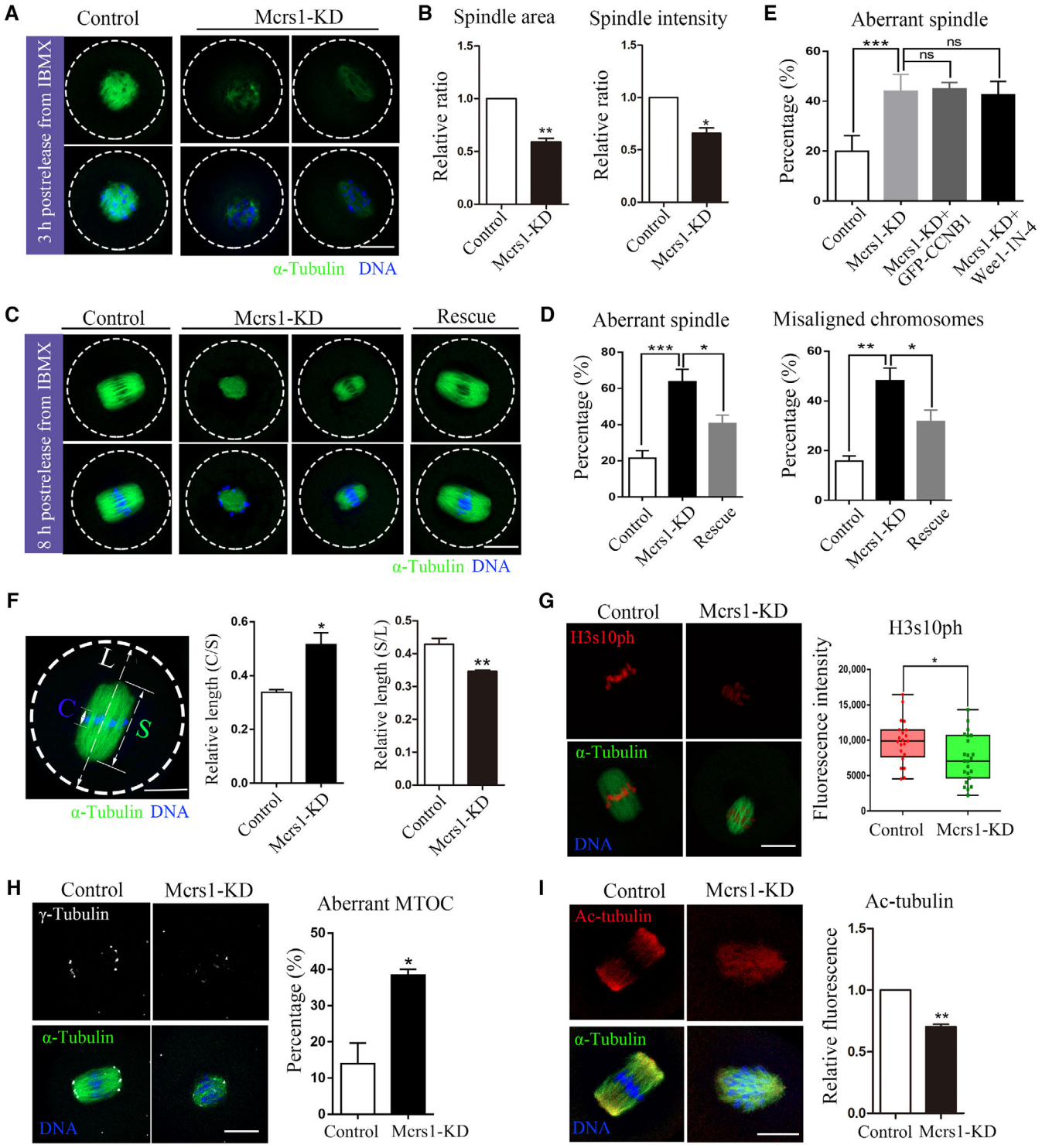

Figure 4.

© 2023 The Authors

Figure 4. Mcrs1 depletion impairs meiotic spindle assembly in oocytes.

A Representative images of spindle assembly at 3-h postrelease from IBMX in control and Mcrs1-KD oocytes. Scale bar, 20 μm.
B The relative area and fluorescence of spindles in control ($n = 82$) and Mcrs1-KD ($n = 73$) oocytes at 3-h postrelease from IBMX. *$P < 0.05$; **$P < 0.01$.
C Representative images of spindle assembly and chromosome alignment at 8-h postrelease from IBMX in control, Mcrs1-KD, and Mcrs1-rescue oocytes. Scale bar, 20 μm.
D Percentages of control ($n = 84$), Mcrs1-KD ($n = 80$), and Mcrs1-rescue ($n = 62$) oocytes with abnormal spindles and misaligned chromosomes. **$P = 0.004$; *$P = 0.014$; ***$P = 0.0009$; *$P = 0.002$.
E Percentages of control ($n = 73$), Mcrs1-KD ($n = 57$), Mcrs1 siRNA + cyclin B1-GFP ($n = 60$), and Mcrs1 siRNA + WEE1-IN-4 ($n = 82$) oocytes with abnormal spindles. ***$P = 0.001$.
F Thickness of the spindle middle plate and relative spindle length. C indicates the maximal span of chromosomes, S indicates the maximal spindle length, and L indicates the oocyte diameter. The histogram shows the C:S and S:L ratios for control ($n = 58$) and Mcrs1-KD ($n = 76$) oocytes at 6 h after GVBD. Scale bar, 20 μm. *$P = 0.018$; **$P = 0.01$.
G Immunofluorescence analysis of H3S10ph and α-tubulin in control and Mcrs1-KD oocytes. Scale bar, 20 μm. The scattergram shows the relative fluorescence intensity of H3S10ph signals in control ($n = 21$) and Mcrs1-KD ($n = 23$) oocytes. *$P = 0.017$.
H Immunofluorescence analysis of γ-tubulin and α-tubulin in control and Mcrs1-KD oocytes. Scale bar, 20 μm. The histogram shows the percentages of control ($n = 55$) and Mcrs1-KD ($n = 63$) oocytes with abnormal γ-tubulin. *$P = 0.014$.
I Immunofluorescence analysis of acetylated tubulin and α-tubulin in control and Mcrs1-KD oocytes. Scale bar, 20 μm. The scattergram shows the relative fluorescence intensity of acetylated tubulin signals in control ($n = 83$) and Mcrs1-KD ($n = 66$) oocytes. **$P = 0.0046$.

Data information: The central band represents the mean. The boxes are representing mean ± SEM and the whiskers are representing Mix to Max. The *P*-values were calculated using unpaired *t*-test. The bars represent the mean ± SEM. The *P*-values were calculated using Student's *t*-test.
Source data are available online for this figure.

Therefore, we concluded that Mcrs1 participates in transcriptional regulation and histone modifications in NSN-type GV oocytes, and it affects cyclin activity for meiotic resumption.

We showed that the transcription factor Mcrs1 regulates spindle assembly during oocyte meiosis I, a cellular process in which transcriptional activity is extremely low. This is consistent with the previous finding that Mcrs1 supports mitotic spindle assembly by localizing to the minus ends of kinetochore microtubules (Petry & Vale, 2011), indicating that the roles of Mcrs1 are conserved in mitotic and meiotic spindles. This suggests that the roles of Mcrs1 in this context are independent of its transcriptional functions because there is almost no transcriptional activity during oocyte meiosis I. We next explored the mechanism by which Mcrs1 affects meiotic spindles in oocytes. CDK1 activity and cyclin B1 accumulation were perturbed in Mcrs1-KD oocytes. CDK1 is reportedly involved in spindle formation and kinetochore-microtubule attachments (Davydenko *et al*, 2013). However, our results showed that the involvement of Mcrs1 in spindle assembly is independent of cyclin. Mcrs1-mediated microtubule assembly in mitosis is dependent on TPX2 (Meunier & Vernos, 2011). Unexpectedly, our results indicated that depletion of Mcrs1 does not affect the localization or expression of TPX2 in mouse oocytes. The localization pattern of Mcrs1 was similar to those of Aurora kinases in meiosis. Aurka reportedly phosphorylates Mcrs1 during mitosis (Meunier *et al*, 2016). In addition, Aurka co-localizes with MTOCs throughout meiosis and is required for recruitment of γ-tubulin, a key MTOC component (Blengini *et al*, 2021), and Aurkc takes over as the predominant chromosomal passenger complex kinase and localizes to chromosomes (Balboula & Schindler, 2014). Aurka deletion results in meiotic spindle defects, similar to the phenotypes observed in the current study (Solc *et al*, 2012). In addition, Aurkc promotes localization of Aurka to spindle poles via competition to ensure that a robust spindle is maintained and meiosis is completed. Aurora kinase B is required to ensure accurate chromosome segregation in oocytes (Nguyen *et al*, 2018). Aurkc is detected at centromeres and along chromosome arms in MI, and its depletion reduces histone H3 phosphorylation and causes chromosome misalignment (Yang *et al*, 2010). This is reminiscent of the misaligned chromosomes

Figure 5. Mcrs1 depletion impairs the activities of Aurora kinases and recruitment of Kif2A in oocytes.

A Immunofluorescence analysis of p-Aurka and α-tubulin in control and Mcrs1-KD oocytes. Scale bar, 20 μm. The arrowhead points to the position of p-Aurka. The histogram shows the percentages of control ($n = 62$) and Mcrs1-KD ($n = 53$) oocytes with abnormal p-Aurka. *$P = 0.02$.
B Immunofluorescence analysis of p-Aurkc and α-tubulin in control and Mcrs1-KD oocytes. Scale bar, 20 μm. The arrowhead points to the position of p-Aurkc. The scattergram shows the relative fluorescence intensity of p-Aurkc signals in control ($n = 33$) and Mcrs1-KD ($n = 27$) oocytes. ***$P = 0.0007$.
C Levels of p-Aurka and p-Aurkc in control and Mcrs1-KD MI oocytes. The blots were probed with anti-p-Aurora A/B/C and anti-actin antibodies.
D Co-IP was performed with an anti-Mcrs1 antibody. The immunoblots of protein precipitates were probed with an anti-Aurka antibody.
E Representative images of the occurrence of GVBD in control, Mcrs1-KD, and Aurka-rescue (Mcrs1 siRNA + Aurka mRNA) oocytes at 12 h following release from IBMX. Scale bar, 100 μm.
F Representative images of spindle assembly and chromosome alignment in control, Mcrs1-KD, and Aurka-rescue oocytes. Scale bar, 20 μm.
G Percentages of control ($n = 92$), Mcrs1-KD ($n = 73$), and Aurka-rescue ($n = 67$) oocytes that underwent PBE. *$P = 0.033$; *$P = 0.018$.
H Percentages of control ($n = 69$), Mcrs1-KD ($n = 76$), and Aurka-rescue ($n = 43$) oocytes with abnormal spindles. *$P = 0.018$; *$P = 0.024$.
I Protein levels of Kif2A in control and Mcrs1-KD MI oocytes. The blots were probed with anti-Kif2A and anti-actin antibodies.
J Protein levels of TPX2 in control and Mcrs1-KD MI oocytes. The blots were probed with anti-TPX2 and anti-actin antibodies.
K Immunofluorescence analysis of Kif2A in control and Mcrs1-KD oocytes. Scale bar, 20 μm. The histogram shows the percentages of control ($n = 50$) and Mcrs1-KD ($n = 61$) oocytes with abnormal Kif2A. **$P = 0.003$.
L Immunofluorescence analysis of TPX2 and α-tubulin in control and Mcrs1-KD oocytes. Scale bar, 20 μm. The scattergram shows the relative fluorescence intensity of TPX2 signals in control ($n = 48$) and Mcrs1-KD ($n = 52$) oocytes.

Data information: The central band represents the mean. The boxes represent mean ± SEM and the whiskers represent Mix to Max. The *P*-values were calculated using unpaired *t*-test. The bars represent the mean ± SEM. The *P*-values were calculated using Student's *t*-test.
Source data are available online for this figure.

© 2023 The Authors

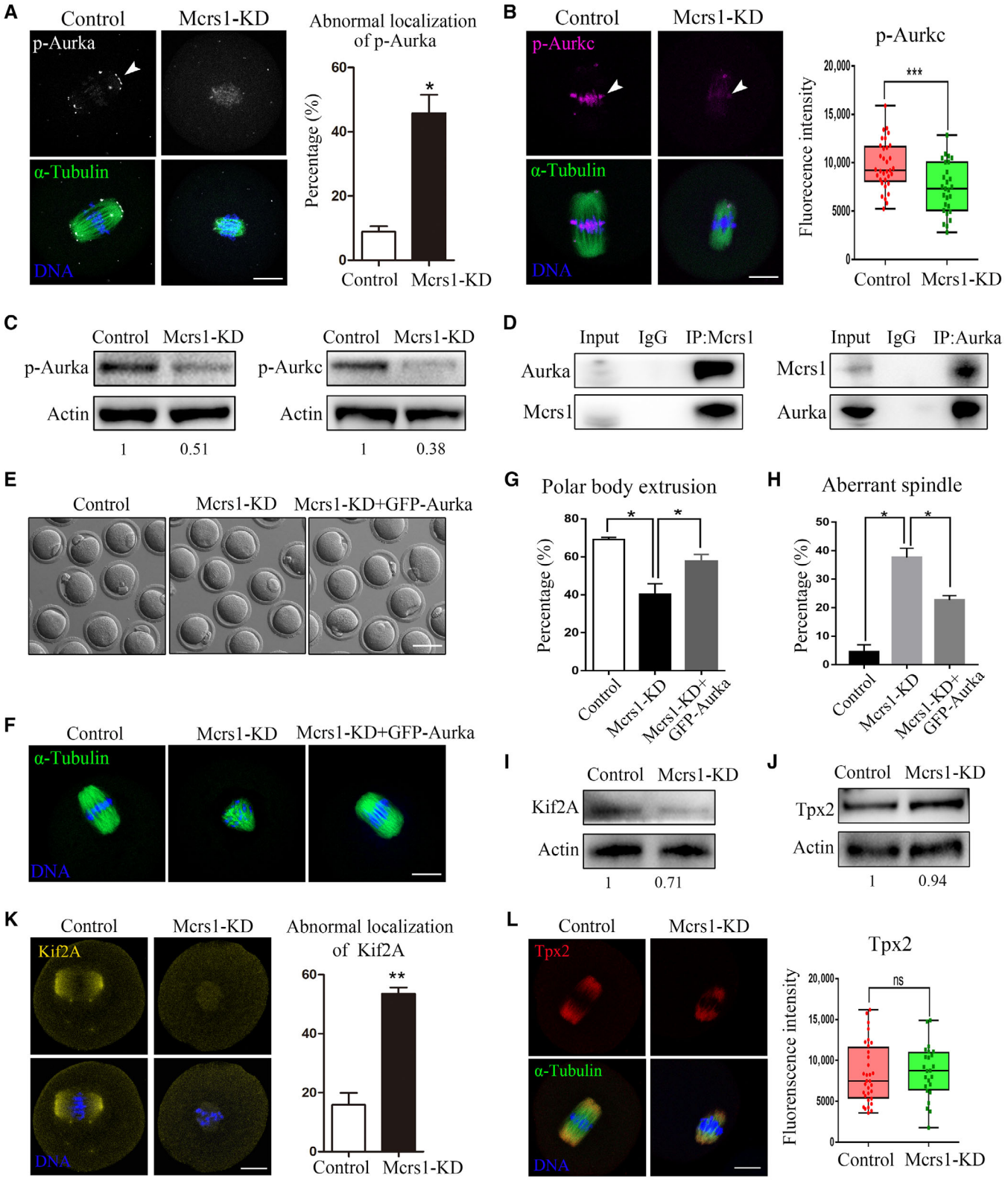

Figure E5.

© 2023 The Authors

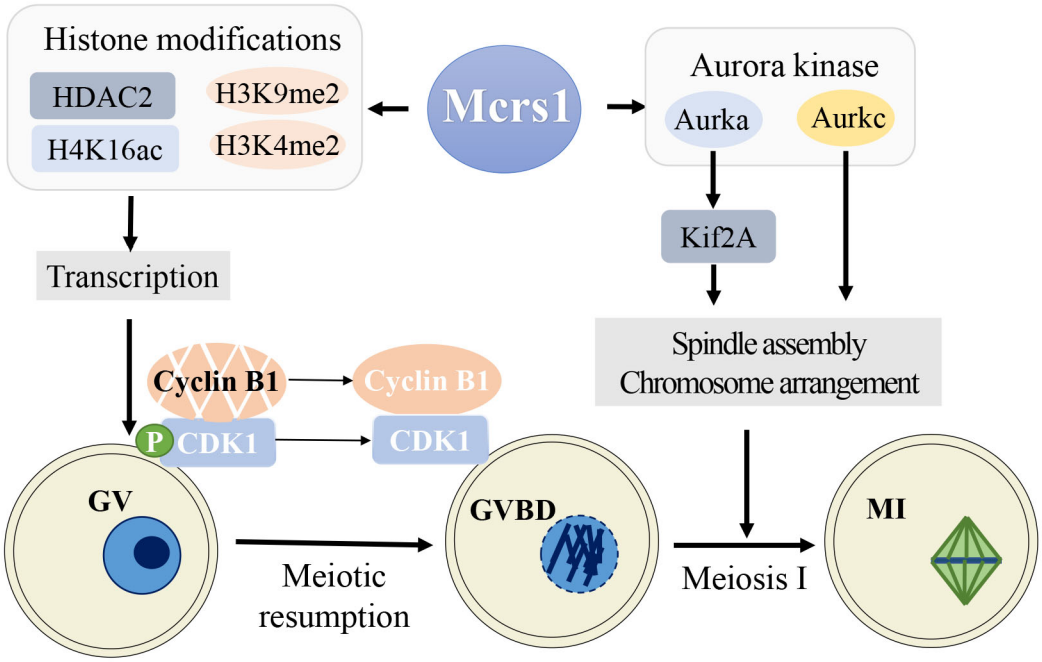

Figure 6. Diagram depicting the roles of Mcrs1 in mouse oocyte meiosis.

Microspherule protein 1 (Mcrs1)-mediated histone modifications are essential for transcriptional regulation in NSN-type GV oocytes, which further determines meiotic resumption. In addition, Mcrs1 regulates microtubule nucleation and spindle assembly by activating Aurora kinases during mouse oocyte meiosis.

and decreased H3S10ph levels in Mcrs1-KD oocytes. Our results showed that Mcrs1 interacted with Aurka and affected expression of Aurka and Aurkc. Aurka has significantly compensatory abilities when the other Aurora kinase homologs are deleted in mouse oocytes (Blengini *et al*, 2021). The rescue of multiple defects in Mcrs1-KD oocytes by expression of exogenous Aurka further confirmed that Mcrs1 is involved in Aurora kinase-mediated spindle assembly. Moreover, the localization and protein expression of Kif2A were abnormal in Mcrs1-KD oocytes. Mcrs1 enables localization of Kif2A to the minus ends of spindle microtubules during mitosis (Yang *et al*, 2019). Given that Aurka also interacts with and phosphorylates Kif2A in mitosis (Jang *et al*, 2009), we concluded that Mcrs1 is crucial for spindle assembly and chromosome alignment via regulating Aurora kinase activity and thus KIF2A expression in meiosis.

In conclusion, we demonstrated that Mcrs1 regulates meiotic resumption by affecting transcription and histone modifications in NSN-type GV oocytes and also interacts with Aurora kinases to regulate spindle assembly and chromosome alignment during MI. Our findings reveal a unique role for Mcrs1 in driving meiotic resumption and progression throughout meiosis I in mouse oocytes.

Materials and Methods

Ethics statement

Animal handling and experimental programs were carried out in accordance with the guidelines of the Animal Research Committee of Nanjing Agricultural University in China, and this study was specifically approved by the Animal Research Committee of Nanjing Agricultural University.

Oocyte collection and *in vitro* culture

All experiments were performed using 4- to 6-week-old female ICR mice and were approved by the Animal Research Committee of Nanjing Agricultural University (China) and conducted in accordance with institutional guidelines. Mice were sacrificed by cervical dislocation. Oocytes were collected from mice and cultured in M2 medium under liquid paraffin oil at 37°C in an atmosphere of air containing 5% CO_2. All reagents and media were purchased from Sigma-Aldrich (St. Louis, MO, USA), unless otherwise stated.

Plasmid construction and mRNA synthesis

The RFP-Mcrs1, GFP-cyclin B1, and GFP-Aurka vectors were generated by Wuhan Gene Create Biological Engineering Co., Ltd. (Wuhan, China). The plasmids were linearized by AvrII, and then mRNAs were synthesized using a HiScribe T7 High Yield RNA Synthesis Kit (NEB, Ipswich, UK), capped with m7G(5)ppp(5)G (NEB), tailed using a Poly(A) Polymerase Tailing Kit (Epicentre, Madison, WI, USA), purified with an RNA Clean & Concentrator Kit (ZYMO RESEARCH, Irvine, CA, USA), and stored at −80°C.

Microinjection of siRNAs and mRNAs

Each fully grown GV oocyte was microinjected with 5–10 pl siRNA or mRNA using a micromanipulator and microinjector (Eppendorf

© 2023 The Authors

AG, Hamburg, Germany) under an inverted microscope (Olympus IX71; Olympus, Tokyo, Japan).

To overexpress RFP-Mcrs1, 400 ng/μl Mcrs1 mRNA solution was injected into the cytoplasm of GV oocytes, and then oocytes were cultured in M2 medium containing 100 mM IBMX for 2 h. To detect RFP-Mcrs1, 300 ng/μl Mcrs1 mRNA solution was injected into the cytoplasm of GV oocytes, and then oocytes were arrested at the GV stage by culture in IBMX-containing medium for 2 h. To overexpress cyclin B1 and Aurka, 500 ng/μl mRNA was microinjected into oocytes, and then oocytes were incubated in IBMX-containing medium for 2 h. Oocytes were injected with the same amount of RNase-free water as a control and treated similarly.

Microspherule protein 1 siRNA (sc-75839; Santa Cruz Biotechnology, Santa Cruz, CA, USA) was injected into the cytoplasm of oocytes to deplete Mcrs1 protein. The concentration of siRNA used for microinjection was 40 μM. The same amount of negative control siRNA was used as a control. Following microinjection, GV oocytes were cultured in M2 medium supplemented with 100 μM IBMX for 24 h and then transferred to IBMX-free M2 medium in order to resume meiosis for subsequent experiments.

Antibodies

Rabbit polyclonal anti-Mcrs1 (11362-1-AP), rabbit polyclonal anti-Kif2A (13105-1-AP), and rabbit polyclonal anti-TPX2 (11741-1-AP) antibodies were purchased from Proteintech (Rosemont, IL, USA). Hoechst 33342 (B2261), an anti-α-tubulin-FITC antibody (F-2168), and a mouse monoclonal anti-acetylated tubulin antibody (T7451) were purchased from Sigma-Aldrich. Mouse monoclonal anti-cyclin B1 (sc-245), rabbit polyclonal anti-CDK1 p34 (sc-12340-R), and mouse monoclonal anti-Mcrs1 (sc-376569) antibodies were purchased from Santa Cruz Biotechnology. Rabbit polyclonal anti-H3K9me2 (ab176882), rabbit monoclonal anti-H4K16ac (ab109463), rabbit monoclonal anti-HDAC2 (ab32117), rabbit monoclonal anti-γ-tubulin (ab179503), and rabbit monoclonal anti-pCDK1(Y15; ab275958) antibodies were purchased from Abcam (Cambridge, UK). Anti-β-actin (4970), rabbit monoclonal anti-H3K4me2 (C64G9), and rabbit monoclonal anti-p-Aurora A/B/C (D13A11) antibodies were obtained from Cell Signaling Technology (Danvers, MA, USA). A rabbit polyclonal anti-H3S10ph antibody (42704) was obtained from GeneTex (Irvine, CA, USA). TRITC-conjugated goat anti-rabbit IgG and FITC-conjugated goat anti-rabbit IgG antibodies were purchased from Zhongshan Golden Bridge Biotechnology (Beijing, China). Horseradish peroxidase-conjugated goat anti-rabbit/mouse IgG (H + L) antibodies were obtained from CWBIO (Beijing, China). Alexa Fluor 594-conjugated goat anti-mouse (A-11005) and Alexa Fluor 488-conjugated goat anti-rabbit (A-11008) antibodies were obtained from Invitrogen (Carlsbad, CA, USA).

EU incorporation assay

Oocytes were cultured in M2 medium containing 100 μM EU for 2 h, fixed, permeabilized, and stained using a Cell-Light EU Apollo488 RNA Imaging Kit (C10316-3; RIBOBIO, China) according to the manufacturer's instructions. Oocytes were imaged using a Zeiss LSM700 confocal microscope.

Immunofluorescence staining and confocal microscopy

Oocytes at specific stages were fixed in phosphate-buffered saline (PBS) containing 4% paraformaldehyde for 30 min, permeabilized in PBS containing 0.5% Triton X-100 for 20 min, blocked in PBS containing 1% bovine serum albumin for 1 h at room temperature, and incubated with primary antibodies. After three washes with PBS containing 0.1% Tween 20 and 0.01% Triton X-100, oocytes were incubated with Alexa Fluor 488- and Alexa Fluor 594-conjugated goat anti-rabbit/mouse IgG secondary antibodies (1:200). Finally, oocytes were incubated with Hoechst 33342 for 20 min to stain chromosomes. Images were acquired using a laser-scanning confocal fluorescence microscope (Zeiss LSM 700 META; Zeiss, Jena, Germany). The primary antibodies used for immunofluorescence staining were anti-α-tubulin-FITC (1:500), anti-H3K9me2 (1:200), anti-H4K16ac (1:100), anti-H3K4me2 (1:200), anti-HDAC2 (1:100), anti-γ-tubulin (1:200), anti-acetylated tubulin (1:500), anti-H3S10ph (1:100), anti-p-Aurora A/B/C (1:100), anti-Kif2A (1:100), and anti-TPX2 (1:100).

Western blotting

Oocytes were lysed by incubation in NuPAGE LDS sample buffer at 98°C for 10 min. Proteins were separated by SDS-PAGE at 160 V for 70 min and then transferred to membranes (Millipore, Billerica, MA, USA) at 20 V for 100 min. Membranes were blocked with Western Rapid Transfer Buffer (P0572; Beyotime, Shanghai, China) for 30 min. Following incubation overnight at 4°C with anti-Mcrs1 (1:500), anti-cyclin B1 (1:1,000), anti-acetylated tubulin (1:2,000), anti-β-actin (1:2,000), anti-CDK1 (1:500), anti-CDC2 p34 (1:500), anti-H3K4me2 (1:500), anti-HDAC2 (1:500), anti-Kif2A (1:500), and anti-TPX2 (1:500) antibodies, membranes were washed thrice with TBST (10 min each) and incubated with horseradish peroxidase-conjugated secondary antibodies at room temperature for 1 h. Finally, membranes were processed using the ECL Plus Western Blotting Detection System Tanon-3900 (Tanon, Shanghai, China).

Co-IP

Ten ovaries were lysed in appropriate lysis buffer for 1 h on ice and centrifuged (12,000 *g* for 10 min), and the supernatant was collected. An anti-Mcrs1 antibody, an anti-Aurka antibody (AA921; Beyotime, Shanghai, China), and Dynabeads Protein G (ThermoFisher Scientific, USA) were incubated together for 3–4 h at room temperature. The beads were washed thrice with lysis buffer to remove nonbound antibodies. The antibody-conjugated Dynabeads were incubated with the supernatant overnight at 4°C. The resultant immune complexes were subjected to Western blotting in order to determine the interaction of proteins. The input was 10 μl of lysate without any antibody and IgG was used as a control antibody.

Mass spectroscopy analysis

In total, 500 μl of ovarian lysate was incubated with anti-Mcrs1 antibody-conjugated beads (or IgG antibody-conjugated beads as a control). The samples were sent to the Wuhan Gene Create Biological Engineering Company for mass spectrometry analysis.

 © 2023 The Authors

Statistical analysis

All experiments were repeated at least three times. Data were analyzed by the *t*-test using the GraphPad Prism 5 software (GraphPad, San Diego, CA, USA) and expressed as mean with standard error of the mean. $P < 0.05$ was considered statistically significant.

Data availability

All data generated or analyzed during this study are included in this published article. This study includes no data deposited in external repositories.

Expanded View for this article is available online.

Acknowledgments
We would like to thank Yuan-Jing Zou, Hao-Lin Zhang, and Meng-Meng Shan for helpful discussion. This work was supported by the National Key Research and Development Program of China (2021YFC2700100) and National Natural Science Foundation of China (32170857).

Author contributions
Jia-Qian Ju: Conceptualization; data curation; formal analysis; investigation; methodology; writing – original draft. **Zhen-Nan Pan:** Resources; data curation; software; formal analysis; methodology. **Kun-Huan Zhang:** Resources; software; methodology. **Yi-Ming Ji:** Resources; software; methodology. **Jing-Cai Liu:** Data curation; software; formal analysis; methodology. **Shao-Chen Sun:** Conceptualization; supervision; funding acquisition; project administration; writing – review and editing.

Disclosure and competing interests statement
The authors declare that they have no conflict of interest.

References

Andersen DS, Raja SJ, Colombani J, Shaw RL, Langton PF, Akhtar A, Tapon N (2010) Drosophila MCRS2 associates with RNA polymerase II complexes to regulate transcription. *Mol Cell Biol* 30: 4744 – 4755

Balboula AZ, Schindler K (2014) Selective disruption of aurora C kinase reveals distinct functions from aurora B kinase during meiosis in mouse oocytes. *PLoS Genet* 10: e1004194

Bao Y, Shen X (2007) INO80 subfamily of chromatin remodeling complexes. *Mutat Res* 618: 18 – 29

Blengini CS, Ibrahimian P, Vaskovicova M, Drutovic D, Solc P, Schindler K (2021) Aurora kinase a is essential for meiosis in mouse oocytes. *PLoS Genet* 17: e1009327

Carabatsos MJ, Combelles CM, Messinger SM, Albertini DF (2000) Sorting and reorganization of centrosomes during oocyte maturation in the mouse. *Microsc Res Tech* 49: 435 – 444

Clift D, Schuh M (2015) A three-step MTOC fragmentation mechanism facilitates bipolar spindle assembly in mouse oocytes. *Nat Commun* 6: 7217

Cui W, Cheong A, Wang Y, Tsuchida Y, Liu Y, Tremblay KD, Mager J (2020) MCRS1 is essential for epiblast development during early mouse embryogenesis. *Reproduction* 159: 1 – 13

Davydenko O, Schultz RM, Lampson MA (2013) Increased CDK1 activity determines the timing of kinetochore-microtubule attachments in meiosis I. *J Cell Biol* 202: 221 – 229

De La Fuente R (2006) Chromatin modifications in the germinal vesicle (GV) of mammalian oocytes. *Dev Biol* 292: 1 – 12

Eymery A, Liu Z, Ozonov EA, Stadler MB, Peters AHFM (2016) The methyltransferase Setdb1 is essential for meiosis and mitosis in mouse oocytes and early embryos. *Development* 143: 2767 – 2779

Garrido A, Kim E, Teijeiro A, Sánchez Sánchez P, Gallo R, Nair A, Matamala Montoya M, Perna C, Vicent GP, Muñoz J *et al* (2022) Histone acetylation of bile acid transporter genes plays a critical role in cirrhosis. *J Hepatol* 76: 850 – 861

Gueth-Hallonet C, Antony C, Aghion J, Santa-Maria A, Lajoie-Mazenc I, Wright M, Maro B (1993) Gamma-tubulin is present in acentriolar MTOCs during early mouse development. *J Cell Sci* 105: 157 – 166

Han SJ, Chen R, Paronetto MP, Conti M (2005) Wee1B is an oocyte-specific kinase involved in the control of meiotic arrest in the mouse. *Curr Biol* 15: 1670 – 1676

Hayashi K, Yoshida K, Matsui Y (2005) A histone H3 methyltransferase controls epigenetic events required for meiotic prophase. *Nature* 438: 374 – 378

Holt JE, Lane SI, Jones KT (2013) The control of meiotic maturation in mammalian oocytes. *Curr Top Dev Biol* 102: 207 – 226

Inoue A, Nakajima R, Nagata M, Aoki F (2008) Contribution of the oocyte nucleus and cytoplasm to the determination of meiotic and developmental competence in mice. *Hum Reprod* 23: 1377 – 1384

Jang C-Y, Coppinger JA, Seki A, Yates JR, Fang G (2009) Plk1 and Aurora a regulate the depolymerase activity and the cellular localization of Kif2a. *J Cell Sci* 122: 1334 – 1341

Jin J, Cai Y, Yao T, Gottschalk AJ, Florens L, Swanson SK, Gutiérrez JL, Coleman MK, Workman JL, Mushegian A *et al* (2005) A mammalian chromatin remodeling complex with similarities to the yeast INO80 complex. *J Biol Chem* 280: 41207 – 41212

Kang MK, Han SJ (2011) Post-transcriptional and post-translational regulation during mouse oocyte maturation. *BMB Rep* 44: 147 – 157

Kim JM, Liu H, Tazaki M, Nagata M, Aoki F (2003) Changes in histone acetylation during mouse oocyte meiosis. *J Cell Biol* 162: 37 – 46

Kim J, Singh AK, Takata Y, Lin K, Shen J, Lu Y, Kerenyi MA, Orkin SH, Chen T (2015) LSD1 is essential for oocyte meiotic progression by regulating CDC25B expression in mice. *Nat Commun* 6: 10116

Ma W, Baumann C, Viveiros MM (2010) NEDD1 is crucial for meiotic spindle stability and accurate chromosome segregation in mammalian oocytes. *Dev Biol* 339: 439 – 450

Ma P, Pan H, Montgomery RL, Olson EN, Schultz RM (2012) Compensatory functions of histone deacetylase 1 (HDAC1) and HDAC2 regulate transcription and apoptosis during mouse oocyte development. *Proc Natl Acad Sci U S A* 109: E481 – E489

MacLennan M, Crichton JH, Playfoot CJ, Adams IR (2015) Oocyte development, meiosis and aneuploidy. *Semin Cell Dev Biol* 45: 68 – 76

Meunier S, Vernos I (2011) K-fibre minus ends are stabilized by a RanGTP-dependent mechanism essential for functional spindle assembly. *Nat Cell Biol* 13: 1406 – 1414

Meunier S, Vernos I (2016) Acentrosomal microtubule assembly in mitosis: the where, when, and how. *Trends Cell Biol* 26: 80 – 87

Meunier S, Shvedunova M, Van Nguyen N, Avila L, Vernos I, Akhtar A (2015) An epigenetic regulator emerges as microtubule minus-end binding and stabilizing factor in mitosis. *Nat Commun* 6: 7889

© 2023 The Authors

Meunier S, Timón K, Vernos I (2016) Aurora-a regulates MCRS1 function during mitosis. *Cell Cycle* 15: 1779 – 1786

Miyara F, Migne C, Dumont-Hassan M, Le Meur A, Cohen-Bacrie P, Aubriot F-X, Glissant A, Nathan C, Douard S, Stanovici A *et al* (2003) Chromatin configuration and transcriptional control in human and mouse oocytes. *Mol Reprod Dev* 64: 458 – 470

Mogessie B, Scheffler K, Schuh M (2018) Assembly and positioning of the oocyte meiotic spindle. *Annu Rev Cell Dev Biol* 34: 381 – 403

Mullen TJ, Davis-Roca AC, Wignall SM (2019) Spindle assembly and chromosome dynamics during oocyte meiosis. *Curr Opin Cell Biol* 60: 53 – 59

Nguyen AL, Drutovic D, Vazquez BN, El Yakoubi W, Gentilello AS, Malumbres M, Solc P, Schindler K (2018) Genetic interactions between the Aurora kinases reveal new requirements for AURKB and AURKC during oocyte meiosis. *Curr Biol* 28: 3458 – 3468

Pan B, Li J (2019) The art of oocyte meiotic arrest regulation. *Reprod Biol Endocrinol* 17: 8

Petry S (2016) Mechanisms of mitotic spindle assembly. *Annu Rev Biochem* 85: 659 – 683

Petry S, Vale RD (2011) A new cap for kinetochore fibre minus ends. *Nat Cell Biol* 13: 1389 – 1391

Ren Y, Busch RK, Perlaky L, Busch H (1998) The 58-kDa microspherule protein (MSP58), a nucleolar protein, interacts with nucleolar protein p120. *Eur J Biochem* 253: 734 – 742

Richani D, Gilchrist RB (2018) The epidermal growth factor network: role in oocyte growth, maturation and developmental competence. *Hum Reprod Update* 24: 1 – 14

Sasaki H, Matsui Y (2008) Epigenetic events in mammalian germ-cell development: reprogramming and beyond. *Nat Rev Genet* 9: 129 – 140

Schmitt A, Nebreda AR (2002) Signalling pathways in oocyte meiotic maturation. *J Cell Sci* 115: 2457 – 2459

Sha Q-Q, Dai X-X, Jiang J-C, Yu C, Jiang Y, Liu J, Ou X-H, Zhang S-Y, Fan H-Y (2018) CFP1 coordinates histone H3 lysine-4 trimethylation and meiotic cell cycle progression in mouse oocytes. *Nat Commun* 9: 3477

Sheikh BN, Guhathakurta S, Akhtar A (2019) The non-specific lethal (NSL) complex at the crossroads of transcriptional control and cellular homeostasis. *EMBO Rep* 20: e47630

Shimono K, Shimono Y, Shimokata K, Ishiguro N, Takahashi M (2005) Microspherule protein 1, mi-2beta, and RET finger protein associate in the nucleolus and up-regulate ribosomal gene transcription. *J Biol Chem* 280: 39436 – 39447

Solc P, Baran V, Mayer A, Bohmova T, Panenkova-Havlova G, Saskova A, Schultz RM, Motlik J (2012) Aurora kinase a drives MTOC biogenesis but does not trigger resumption of meiosis in mouse oocytes matured *in vivo*. *Biol Reprod* 87: 85

Sun QY, Miao YL, Schatten H (2009) Towards a new understanding on the regulation of mammalian oocyte meiosis resumption. *Cell Cycle* 8: 2741 – 2747

Szollosi D, Calarco P, Donahue RP (1972) Absence of centrioles in the first and second meiotic spindles of mouse oocytes. *J Cell Sci* 11: 521 – 541

Tachibana M, Nozaki M, Takeda N, Shinkai Y (2007) Functional dynamics of H3K9 methylation during meiotic prophase progression. *EMBO J* 26: 3346 – 3359

Tan J-H, Wang H-L, Sun X-S, Liu Y, Sui H-S, Zhang J (2009) Chromatin configurations in the germinal vesicle of mammalian oocytes. *Mol Hum Reprod* 15: 1 – 9

Tsai M-Y, Zheng Y (2005) Aurora a kinase-coated beads function as microtubule-organizing centers and enhance RanGTP-induced spindle assembly. *Curr Biol* 15: 2156 – 2163

Yang K-T, Li S-K, Chang C-C, Tang C-JC, Lin Y-N, Lee S-C, Tang TK (2010) Aurora-C kinase deficiency causes cytokinesis failure in meiosis I and production of large polyploid oocytes in mice. *Mol Biol Cell* 21: 2371 – 2383

Yang H, Zhang F, Huang C-J, Liao J, Han Y, Hao P, Chu Y, Lu X, Li W, Yu H *et al* (2019) Mps1 regulates spindle morphology through MCRS1 to promote chromosome alignment. *Mol Biol Cell* 30: 1060 – 1068

Zhang C, Chen Z, Yin Q, Fu X, Li Y, Stopka T, Skoultchi AI, Zhang Y (2020) The chromatin remodeler Snf2h is essential for oocyte meiotic cell cycle progression. *Genes Dev* 34: 166 – 178

 © 2023 The Authors